Biophysical Journal Volume 108 June 2015 2670–2679

Article

Skin Lipids: Localization of Ceramide and Fatty Acid in the Unit Cell of the Long Periodicity Phase

Enamul H. Mojumdar,[1] Gert S. Gooris,[1] David J. Barlow,[2] M. Jayne Lawrence,[2] Bruno Deme,[3] and Joke A. Bouwstra[1,*]

[1]Leiden Academic Centre for Drug Research, Department of Drug Delivery Technology, Gorlaeus Laboratories, University of Leiden, Leiden, the Netherlands; [2]Pharmaceutical Science Division, King's College London, London, United Kingdom; and [3]Institute Laue-Langevin, Grenoble, France

ABSTRACT The lipid matrix of the skin's stratum corneum plays a key role in the barrier function, which protects the body from desiccation. The lipids that make up this matrix consist of ceramides, cholesterol, and free fatty acids, and can form two coexisting crystalline lamellar phases: the long periodicity phase (LPP) and the short periodicity phase (SPP). To fully understand the skin barrier function, information on the molecular arrangement of the lipids in the unit cell of these lamellar phases is very desirable. To determine this arrangement in previous studies, we examined the molecular arrangement of the SPP. In this study, neutron diffraction studies were performed to obtain information on the molecular arrangement of the LPP. The diffraction pattern reveals nine diffraction orders attributed to the LPP with a repeating unit of 129.4 ± 0.5 Å. Using D_2O/H_2O contrast variation, the scattering length density profiles were calculated for protiated samples and samples that included either the perdeuterated acyl chain of the most abundant ceramide or the most abundant perdeuterated fatty acid. Both perdeuterated chains are predominantly located in the central part of the unit cell with substantial interdigitation of the acyl chains in the unit cell center. However, a fraction of the perdeuterated chains is also located near the border of the unit cell with their acyl chains directing toward the center. This arrangement of lipids in the LPP unit cell corresponds with the location of their lipid headgroups at the border and also inside of the unit cell at a well-defined position (±21 Å from the unit cell center), indicative of a three-layer lipid arrangement within the 129.4 ± 0.5 Å repeating unit.

INTRODUCTION

Neutron diffraction provides a sensitive and versatile technique to probe the structure of biological membranes. The technique relies on the large difference between the coherent scattering amplitudes of hydrogen and deuterium, a quality that makes it selectively advantageous over other methods such as x-ray diffraction. Using neutron diffraction, the scattering length density profiles are obtained by means of Fourier reconstructions to determine the distribution of membrane lipids along the normal to the membrane plane (1–10). In the studies reported here, we embarked upon a journey to examine a lamellar structure that is exclusively present in the superficial layer of the skin. The lipids in this layer mainly comprise cholesterol (CHOL), free fatty acids (FFAs), and members of the sphingolipid family, namely ceramides (CERs) (11–14).

This superficial layer of the skin is referred to as the *stratum corneum* (SC) and provides a physical barrier to prevent the body from experiencing desiccation. The CHOL, CERs, and FFAs in the SC are located between dead keratin-containing cells (referred to as corneocytes); the composite layer is thus presented as a brick-and-mortar structure. The partitioning of many compounds into the corneocytes is limited (15,16). This is due to their cornified envelope wrapping around these dead cells. Consequently, the tortuous intercellular domains filled by the lipids form the most important pathway for penetration of substances across the skin (17). Therefore, to unravel the natural function of the skin, i.e., the barrier function, it is crucial to have detailed knowledge on the molecular organization of this intercellular lipid matrix.

When focusing in more detail on the lipid composition, the CERs are characterized by the presence of long hydrocarbon chains (acyl chains chemically linked to sphingoid bases). The FFAs present in the human SC are mainly saturated and range in chain length from C14 to C34 (18,19). The CERs can vary in their headgroup architecture and in the number of carbon atoms in the acyl chain and sphingoid base. To date, 14 different subclasses of CERs have been identified in human SC (12,13,20,21). CERs are key players in the molecular organization of the SC (22,23).

In concert, the three main lipid classes adopt lamellar phases that are characteristic of the SC. In human and pig SC, two coexisting crystalline lamellar phases are presently referred to as the long periodicity phase (LPP) and short periodicity phase (SPP), with repeat distances of ~130 and 60 Å, respectively (24,25). It has been reported that the LPP plays a crucial role in maintaining the skin barrier: the absence of the LPP in the SC lipid model membranes

Submitted September 4, 2014, and accepted for publication April 21, 2015.

*Correspondence: bouwstra@chem.leidenuniv.nl

Editor: Ka Yee Lee.

0006-3495/15/06/2670/10 $2.00

http://dx.doi.org/10.1016/j.bpj.2015.04.030

drastically reduces the lipid barrier function. Similarly a reduced level of lipids forming the LPP is thought to reduce the skin barrier in diseased states, for example, in atopic dermatitis and in dry skin (26–29). To understand the role of the lipid classes in the formation of the lamellar phases and thus their function in the skin barrier, it is important to unravel the molecular arrangement in the unit cells of these lamellar phases. In two previous studies, we focused on the molecular arrangement of the CERs, CHOL, and FFAs in the unit cell of the SPP (27,30). The aim of this study is to solve the molecular arrangement of the lipids present in the LPP.

Previously, using x-ray diffraction techniques, we were able to determine the electron density profiles in the unit cell of the LPP. These studies indicated that, unlike phospholipid lamellae in general, but also unlike the SPP bilayer arrangements, the unit cell of the LPP consists of a trilayer arrangement (31,32).

Structure determination by x-ray diffraction offers only limited utility for probing the lipid organization within the LPP—because of the low level of hydration and low contrast of the system, but the obtained electron density profiles of the unit cell can be considered as a fingerprint of the lipid arrangement in the unit cell. Neutron diffraction measurements of the LPP lamellae offer significantly greater resolution in terms of D_2O/H_2O contrast. Taking advantage of contrast variation and selective deuteration, information can be obtained about the location and molecular arrangement of the lipid molecules in the unit cell of the LPP. By this means, we investigated the highly abundant subclasses of lipids present in the mixture, namely a nonhydroxy acyl chain linked to a sphingoid base (CER NS C24) with the acyl chain deuterated and the FFA C24 (lignoceric acid) perdeuterated. These lipids form at ~30 mol % of their corresponding CER and FFA classes. Using neutron diffraction in combination with D_2O/H_2O contrast variation, first the water phase signs of the lipid mixtures were selected. Subsequently, the neutron scattering length density profiles (SLDs) were constructed for the protiated and the deuterated mixtures and the location of the CER NS and FFA C24 lipids were determined. Finally, the water profile based on the lipid headgroups in the unit cell of the LPP together with the positions of the CER NS and FFA C24 lipids were determined.

MATERIALS AND METHODS

Materials

Five subclasses of synthetic CERs were used in our studies. These are 1) the ester linked omega-hydroxyl acyl chain (abbreviation EO, 30 carbons in the acyl chain (C30)) with a sphingosine chain (abbreviation S, C18) referred to as CER EOS (C30); 2) a nonhydroxy acyl chain (abbreviation N, C24) linked to a sphingosine base (C18) referred to as CER NS (C24); 3) a nonhydroxy acyl chain (C24 or C16) linked to a phytosphingosine base (abbreviation P) referred to as CER NP (C24) and CER NP (C16), respectively; 4) an α-hydroxy chain (abbreviation A) linked to a sphingosine base referred to as CER AS (C24); and 5) an α-hydroxy acyl chain (C24) linked to a phytosphingosine base referred to as CER AP (C24). The number given in parentheses indicates the number of carbon atoms present in the acyl chain of the CERs. The molecular structure of the synthetic CERs are provided in Fig. 1. All the CERs were generously provided by

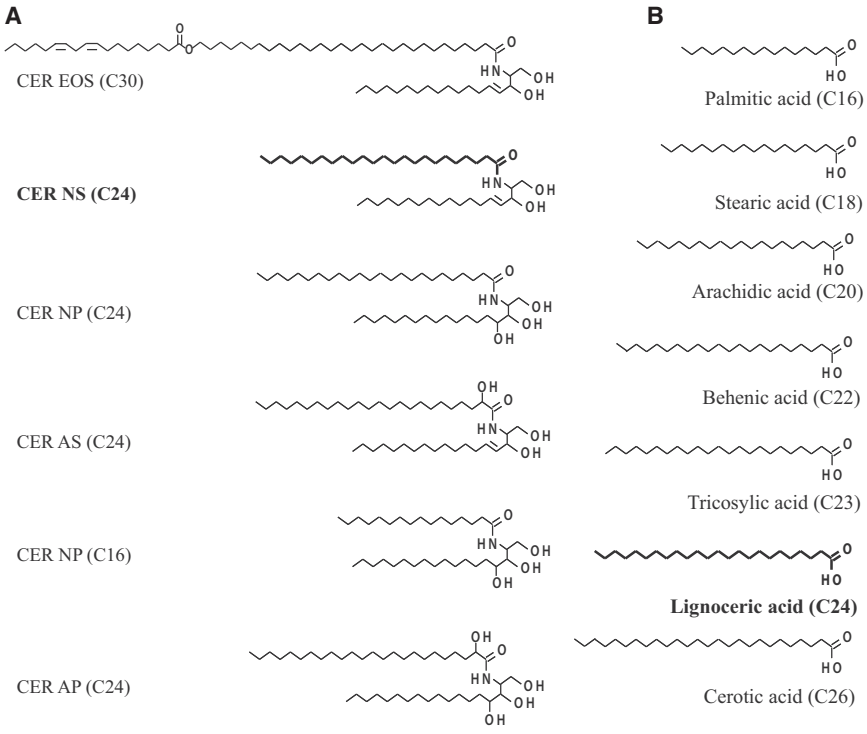

FIGURE 1 Molecular structure of the various (*A*) CER subclasses and (*B*) FFAs used in this study. (*Bold*) CER NS (C24) and FFA lignoceric acid (C24:0) were used to prepare the deuterated lipid mixtures as explained in the Materials and Methods. In preparing the protiated sample, all these lipids were used in their protiated form.

Evonik (Essen, Germany). Palmitic acid (C16:0), stearic acid (C18:0), arachidic acid (C20:0), behenic acid (C22:0), tricosanoic acid (C23:0), lignoceric acid (C24:0), cerotic acid (C26:0), CHOL, and deuterated water were obtained from Sigma-Aldrich Chemie (Schnelldorf, Germany). Deuterated CER NS (C24) and FFA C24:0 were obtained from Arc Laboratories B.V. (Apeldoorn, the Netherlands). The molecular structure of the FFAs is also shown in Fig. 1. Silicon substrates were obtained from Okmetic (Vantaa, Finland). All solvents used were of analytical grade and supplied by Labscan (Dublin, Ireland). The water was of Millipore quality produced by a Milli-Q water filtration system (Millipore, Billerica, MA) with a resistivity of 18 MΩ.cm at 25°C.

Sample preparation method

The lipid mixtures consisted of CERs, CHOL, and FFAs in an equimolar ratio. The CER subclasses with their chain length and molar ratios used in this study are given in Table 1. This ratio resembles very closely the CER composition reported in the pig SC (33), except that the CER EOS is present at an increased level (~10 mol % in case of pig SC versus 40 mol % in this study). In all of these CERs, the sphingoid base has a chain length of C18. The FFA composition was prepared from seven FFA subclasses. Their name, chain length, and molar ratios are also provided in Table 1. The composition of the FFA mixture is based on the FFA chain-length distribution reported for human SC (34). For preparing the deuterated lipid mixtures, the protiated CER NS and FFA C24 were replaced by their deuterated counterparts. In the case of CER NS, only the acyl chain was deuterated whereas the FFA C24 was perdeuterated (see Fig. 1, *bold marked*). A total of three different model lipid membranes were prepared. The composition of these model lipid mixtures with their molar ratios and the total number of deuterated atoms per molecule are provided in Table 2. For preparing the lipid mixtures, the appropriate amount of lipids was dissolved in chloroform/methanol (2:1 v/v) solution at 10 mg/mL concentration. Subsequently the lipids were sprayed on a silicon substrate in an area of 1.2 × 4.0 cm^2 using a Camag Linomat IV sample applicator (Muttenz, Switzerland). The temperature during the spray was 25°C and spraying rate was set to 5 μL/min. During spraying, the solvent was evaporated by a gentle flow of nitrogen gas. Ten milligrams, total, of lipids were sprayed on the substrate.

TABLE 1 The various lipid classes and their corresponding molar ratios used to prepare the mixtures for neutron diffraction experiments

Description	Synthetic Lipids	Molar Ratio (%)
CER name and chain length	CER EOS (C30)	13.3
	CER NS (C24)	**12**
	CER NP (C24)	3.7
	CER AS (C24)	1
	CER NP (C16)	2
	CER AP (C24)	1.3
	CERmix	Total 33.3
CHOL	**CHOL (C27)**	**33.3**
FFA name and chain length	palmitic acid (C16)	0.6
	stearic acid (C18)	1.3
	arachidic acid (C20)	2.6
	behenic acid (C22)	14.2
	tricosylic acid (C23)	1.7
	lignoceric acid (C24)	**11.5**
	cerotic acid (C26)	1.4
	FFA	Total 33.3
Total	CER:CHOL:FFA	100

The lipids provided in bold are those that are used in protiated and deuterated form to determine their localization in the unit cell.

In order to maintain a homogeneous temperature environment during the equilibration method, after spraying, the lipid films were placed in an aluminum chamber. Subsequently, the chamber was filled with argon gas to avoid lipid oxidation at elevated temperatures. The sample was then equilibrated close to the melting temperature at ~68–70°C for ~12 min and gradually cooled to room temperature. The samples were then hydrated with at least three different D_2O/H_2O mixtures selected from the ratios 8:92, 50:50, or 67:33 and 100:0 (v/v) at 100% relative humidity (RH). The sequence of D_2O/H_2O ratios was randomized. For the first time, the samples were hydrated for ~15 h at 37°C and with the RH maintained at 100% before the neutron diffraction measurements. After measuring with that particular D_2O/H_2O mixture, the samples were subsequently allowed to hydrate for ~12 h at 37°C using a different D_2O/H_2O mixture.

Neutron diffraction experiment

All the neutron diffraction experiments were performed on the D16 cold neutron diffractometer of the Institute Laue-Langevin located in Grenoble, France. The wavelength of neutron beam was 4.75 Å and all the samples were measured in the reflection mode. The sample/detector distance was kept at 85 cm. The samples were mounted on a goniometer placed in an aluminum chamber. The temperature of the chamber was maintained at 25°C throughout the measurements. While measuring the sample hydrated at a particular D_2O/H_2O, the bottom of the chamber was filled with the same D_2O/H_2O to maintain a constant 100% RH. The measurement time per sample varied between 10 and 12 h depending on the signal/noise. A position-sensitive two-dimensional ^3He detector with an area of 320 × 320 mm and a spatial resolution of 1 × 1 mm was used to record the neutron scattering density. The order of measurements of the samples with specific D_2O/H_2O ratios was randomized.

Data analysis

Sensitivity differences on the detector surface were corrected by using water calibration measurements. In order to increase the signal/noise, a background measurement of the empty chamber was also performed and subtracted from each sample measurement. For the data analysis, the software LAMP (Institute Laue-Langevin) was used (35). During the measurements, the sample was rotated in steps of 0.1° from 0 to 10.5° to cover all the nine diffraction orders and the detector images were taken at each step. The two-dimensional detector data was integrated in the vertical direction, resulting in a one-dimensional diffraction pattern of scattering intensity as a function of the scattering angle (2θ). The scattering angle 2θ is converted to the scattering vector q as

$$q = \frac{4.\pi.\sin\theta}{\lambda}. \quad (1)$$

In this equation, θ is the Bragg angle and λ is the wavelength of the neutron beam. A typical one-dimensional diffraction plot of intensity versus q is provided in Fig. 2.

The repeat distance (d) of the unit cell was calculated from the positions of a series of equidistant peaks attributed to the lamellar phase (q_h) by

$$d = \frac{2.\pi.h}{q_h}, \quad (2)$$

where h represents the diffraction order. All diffraction peaks were fitted as Gaussians ($\int(x)$),

$$\int(x) = ae^{-\frac{(x-\mu)^2}{2\sigma^2}} + c, \quad (3)$$

TABLE 2 The lipid composition with their deuterated mol % and the total number of deuterated atoms per lipid molecule for various compositions forming an LPP, measured with neutron diffraction

Lipid Model Type	Lipid Composition and Molar Ratio (Equimolar)	Deuterated mol %	Number of Deuterated Atoms per Molecule	Repeating Unit D (Å)
CER^{PRO}	CERmix[a]/CHOL/FFA	0	0	129.4 ± 0.6
$CER^{DCER\ NS}$	CERmix (CER NS)/CHOL/FFA	12	47	129.4 ± 0.4
$CER^{DFFA\ C24}$	CERmix/CHOL/FFA (C24:0)	11.5	47	129.3 ± 0.6

The repeat distance with their uncertainties of all the lipid mixtures is also presented.
[a]The CERmix consisted of CER EOS C30, CER NS C24, CER NP C24, CER AS C24, CER NP C16, and CER AP C24 in a 13.3:12:3.7:1:2:1.3 molar ratio, as presented in Table 1.

where c is considered the offset for the baseline correction. The structure factor amplitude $|F_h|$ of each diffraction order was then calculated from the Gaussian peak height (I_h) by using the formula

$$|F_h| = A_h\sqrt{L.I_h}. \quad (4)$$

Here, L represents the Lorentz correction. The appropriate values were calculated for all the mixtures and applied to correct for the intensities. A_h is the correction factor for sample absorption, which was calculated using the formula (9)

$$A_h = \frac{1}{\sqrt{\frac{\sin\theta}{2\ \mu l}\left(1 - e^{\frac{-2\ \mu l}{\sin\theta}}\right)}}. \quad (5)$$

In this equation, μ represents the linear attenuation coefficient and l is the thickness of the lipid film. The densities of the various lipid mixtures were calculated by taking into consideration the number of water molecules (two water molecules per lipid molecule) as determined previously (27). Subsequently, the thickness of the membrane (l) was calculated using the density of the lipid membrane in combination with the amount of lipid materials (10 mg) and the area of the spraying membrane (4.8 cm^2), which is ~24 μm. Later, the attenuation coefficient (μ) values were calculated by using the known lipid densities and the chemical composition of the lipid films in combination with the wavelength of the neutrons (36). The error in the structure factors by D_2O/H_2O exchange was calculated from the deviation of the fitted regression lines and is shown in Table S1 in the Supporting Material.

When considering the unit cell of the LPP as centrosymmetric, the structure factor phase signs would be either 0 or π. In that case, the structure factor amplitudes change linearly with increasing the D_2O/H_2O (9). If we assumed that in our lipid mixture, the water is located near the headgroups at the boundaries of the unit cell, the phase signs of the structure amplitudes of water would be $-+-+-+-+-$ for the first nine diffraction orders. This results in a water distribution profile that is in agreement with the previously reported electron density profile (32). A more detailed explanation about the choice of the phase signs is provided in the Results. In addition, the water-layer structure factors are defined as the structure factors at 100% D_2O minus the structure factors at 8% D_2O. Using this information, the structure factor phase signs for both protiated mixture and mixtures containing the deuterated lipids could then be determined from the linear plot of the structure factors versus D_2O/H_2O. This was done in such a way that the difference between 100 and 8% D_2O gives the correct phase sign for the water-layer structure factor at that particular diffraction order. This procedure was carried out for both protiated and deuterated samples. A more detailed description is given elsewhere (8,9,37).

Finally, the SLD profile across the unit cell $\rho(x)$ was calculated by Fourier reconstructions:

$$\rho(x) = F_0 + 2\sum_{h=1}^{h_{max}} F_h \cos\left(\frac{2.\pi.h.x}{d}\right). \quad (6)$$

Here, x is the direction normal to the unit cell surface and $x = 0$ is the center of the unit cell. The value F_0 describes the average scattering density per unit volume and has to be calculated to put the data on an absolute scale. The term F_0 was calculated by using the chemical composition and the mass density of the sample (5,38). The level of CHOL dissolved in the LPP is ~20 mol % of the total lipid mixture (unpublished work); therefore this level was used to determine the F_0 value. To obtain the uncertainty in the F_0 value, we calculated F_0 when CHOL level varied between 10 and 25 mol %. It appeared that the effect on the F_0 value was negligible. The data were then put on a relative-absolute scale (6,30,39,40) using the following procedure: The known neutron SLDs of deuterium and hydrogen were used to scale the differences in such a way that the area differences between the SLDs are equal to the SLD of the deuterium label, for example, a 47-deuterium difference in case of DFFA C24. The difference density profile was then constructed by subtracting the protiated profile from the deuterated profile.

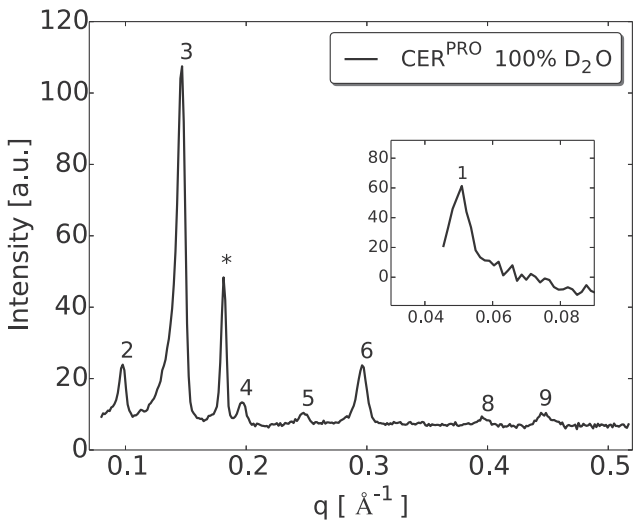

FIGURE 2 One-dimensional neutron diffraction plot of the LPP mixture prepared with protiated lipids (CER^{PRO}) and hydrated at 100% D_2O/H_2O. Various diffraction orders of the LPP lipid lamellae captured from the measurements are indicated (*Arabic numbers*) as well as the CHOL peak (*asterisk*). (*Inset*) The first-order diffraction pattern of the LPP measured at different detector positions to accommodate the other orders to fit in only one detector position.

RESULTS

Neutron diffraction pattern

The neutron diffraction pattern of the three different model membrane mixtures studied show at least nine diffraction

orders attributed to the LPP. A typical one-dimensional diffraction pattern of intensity versus q plot for CER^{PRO} mixture is provided in Fig. 2, showing the various diffraction orders. All diffraction peaks show a slight peak asymmetry due to the large size of the sample in comparison to the distance to the detector. This is most clearly visible for high-intensity peaks at lower q values. No additional phases were observed apart from crystalline CHOL domain. The reflection from the crystalline CHOL peak is observed at $q = 0.18$ Å and does not interfere with the diffraction orders of the LPP. The one-dimensional diffraction plots for the $CER^{DCER\ NS}$ and $CER^{DFFA\ C24}$ mixtures are provided in the Fig. S1 in the Supporting Material.

The repeat distance of all the samples was calculated from the series of equidistant peaks using known q values of the peak positions obtained by a least-square fitting and is provided in Table 2 with their uncertainties. The mean repeat distance of all the samples was calculated to be 129.4 ± 0.5 Å. The mosaic spreads of the lipid lamellae were determined from the neutron rocking curves by calculating the full width at half-maximum of a Gaussian fit and appeared to be ~0.19 ± 0.03°.

Hydration levels of the LPP model mixture

When hydrating the lipid mixtures, only a small increase in the level of hydration was observed, ~2 water molecules per lipid molecule (27). Therefore, when increasing the D_2O/H_2O ratio, only a moderate increase in the neutron scattering signal was noticed, as shown in Fig. 3. However, the signal/noise in our neutron diffraction measurements was sufficient to discriminate between the protiated and the partly deuterated mixtures.

Determination of the phase signs

To determine the water phase signs of the amplitudes of the different diffraction orders, the contrast variation method was used. If we assume that the headgroups are located close to the boundary of the unit cell, the H_2O should be located close to the headgroup regions and thus also close to the unit cell boundaries. As a result, it is expected that the absolute values of the structure factors will increase when gradually increasing the D_2O/H_2O. On the assumption that water is located in the headgroup regions, in our phase-determining procedure, we systematically varied the phase signs of the various diffraction orders, initially for the first six orders. After having selected those phase-sign combinations that resulted in the most realistic water profiles, in the next step we varied systematically the remaining three phase signs (seven up to nine orders). When assuming the water is located at the boundary of the unit cell at the positions of the headgroups, the most realistic phase signs of water we selected is contained in the combination $-+-+-+-+-$ for the first nine diffraction orders. Combination of these phase signs with the absolute values of the Fourier amplitudes resulted in the location of water not only at the boundary of the unit cell (two regions), but also at two regions inside the unit cell at a position of ~20 Å from the unit cell center. Considering the location of water in these four regions, the water profile was fitted assuming a Gaussian distribution, which results in the similar phase signs (Fig. S2). When changing one of the phase signs of the weak diffraction orders (i.e., fourth, fifth, eighth orders), the change in the net water distribution profile is minor because the contribution of these phase signs to the water SLD is limited (Fig. S3 *A*). On the contrary, when changing one of the high intensity phase signs (i.e., second, third, sixth orders), a different water profile is observed (see Fig. S3 *B*), resulting in an unrealistic water distribution. This is the case for changing each of the phase signs of the high-intensity diffraction peaks. The phase signs of the weak-intensity peaks are with some uncertainty, but do not really contribute to the overall SLD profiles.

The next step was to calculate the phase signs of the various diffraction orders of the LPP, keeping the difference between the structure factors of 100% D_2O and 8% D_2O in agreement with the correct phase signs for the water (Fig. 3). The linear fit of the structure factors with respect to the different D_2O/H_2O ratios demonstrate that the SLD profile

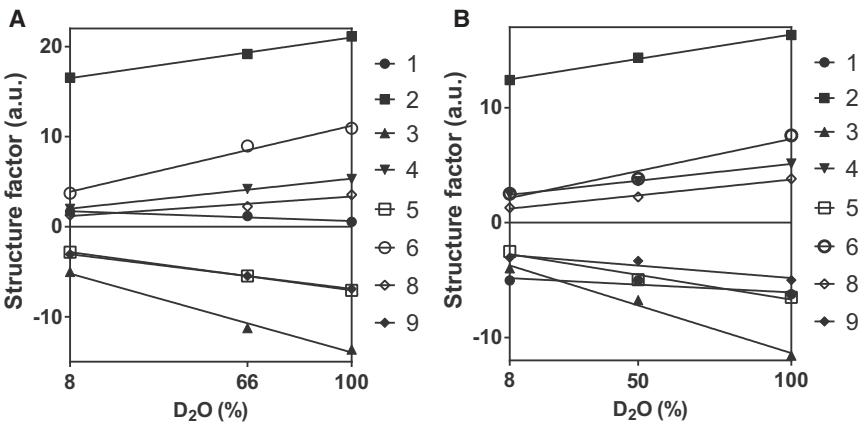

FIGURE 3 Linear fitting of the relative structure factor amplitudes as a function of D_2O/H_2O ratio for all the different diffraction orders of the LPP lipid membrane for (*A*) $CER^{DCER\ NS}$ mixture and (*B*) $CER^{DFFA\ C24}$ mixture. The numbers in the plots indicate the various diffraction orders.

is centrosymmetric. The structure factor amplitudes with their uncertainties and the corrected phase sign assignments for various diffraction orders at different D_2O/H_2O ratios are provided in Table S1.

Note here that systematic consideration was given to all other possible phase sign combinations (as detailed in the Supporting Material), and by this means established that the combination determined as described above, although not uniquely defined, is correct in all essential details, giving confidence that the LPP model reported here is accurate and reliable.

Neutron SLD profiles of the model membrane

The neutron SLD profiles in the unit cell of the protiated and partly deuterated samples were then constructed using the phase signs in combination with the structure factors by using Eq. 6. The profiles constructed at 8 and 100% D_2O/H_2O for the CER^{PRO} mixture are provided in Fig. 4. The difference between the 100 and 8% D_2O/H_2O indicated the water profile. From the water profile (Fig. 4, *bottom*), four distinct regions of elevated scattering density are observed—two at the border, and two inside of the unit cell, indicating the position of the hydrophilic headgroups in these regions. The headgroup regions were fitted assuming Gaussian distributions in order to determine their exact position in the unit cell. The results show that the outer headgroup regions are located at 64.7 ± 0.4 Å from the center of the unit cell, whereas the second submaxima are located at 21 ± 0.3 Å from the unit cell center, indicating the water hydrations in these regions when considering the D_2O/H_2O contrast.

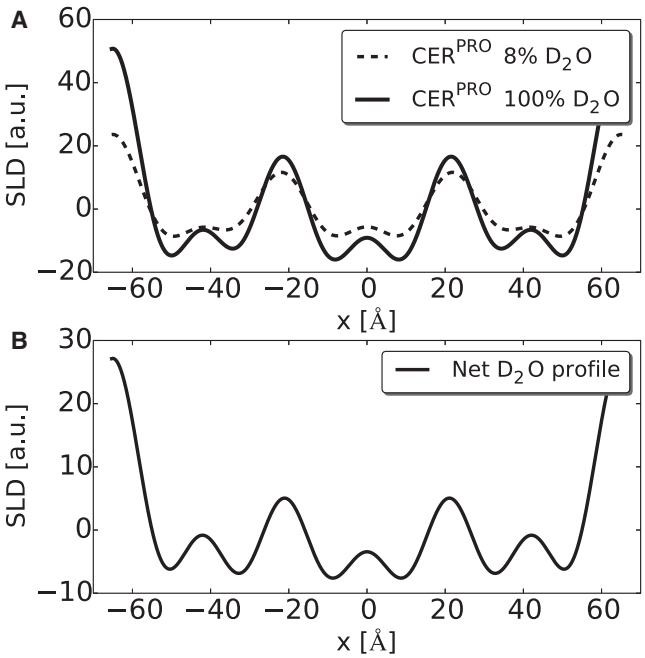

FIGURE 4 The relative SLD profiles of the CER^{PRO} mixture hydrated and measured at 8% (*A*, *dashed line*) and 100% D_2O (*A*, *solid line*) with neutron diffraction at 100% RH. (*B*, *solid line*) Difference profile showing the water SLD. The four headgroup regions in the water profile are clearly visible, indicating a three-layer arrangement in the LPP.

The SLD profiles of the unit cell of the LPP for the $CER^{DCER\ NS}$ or $CER^{DFFA\ C24}$ mixture are provided in Fig. 5. The difference density profiles for the unit cell of the $CER^{DCER\ NS}$ and the $CER^{DFFA\ C24}$ were obtained by subtracting the density profile of the CER^{PRO} either from the $CER^{DCER\ NS}$ profile or from the profile of $CER^{DFFA\ C24}$ (Fig. 5, *bottom*). The difference density profiles indicate the position of deuterated CER NS and deuterated FFA C24 in the LPP unit cell. From the difference density profile, it is evident that the CER NS and FFA C24 are located in the central part of the unit cell. However, an increment in the density near the unit cell border indicates that a proportion of CER NS and FFA C24 are also located close to the outer border of the unit cell.

DISCUSSION

The lipids present in the SC form two crystalline lamellar phases, the LPP and SPP (24,25), which contribute prominently to the skin barrier function. This is why it is crucial to obtain more information on the arrangement of the lipids within the unit cells of these phases. Previously, using neutron diffraction we were able to determine the molecular arrangement of the most abundant lipid molecules present in the unit cell of the SPP (27,30). Based on these calculations, a detailed molecular model for the SPP has been proposed in which the CER NS hydrocarbon chains are interdigitating and the short length of CHOL compensates for the extended FFA having a chain length of 24 carbon atoms. Studies are documented in the literature focusing on the phase behavior of lipid mixtures including 3–5 lipid components (1–3,41). Although these mixtures are often referred to as SPP, their repeat distances are nevertheless somewhat smaller than typical SPP repeat distance of between 50 and 60 Å. In a few studies, CER EOS was also present in the lipid mixtures. Despite the presence of CER EOS, these lipid mixtures do not form the LPP or require a hydrated state of the lipids to form the LPP—a situation not anticipated in our previous studies (3,41,42). Perhaps a mismatch in the chain length of CERs and/or FFA, a different ceramide composition, and/or a difference in thermal history may contribute to a reduced formation or even the absence of the LPP (43).

Furthermore, some of these lipid mixtures showed multiple lamellar phases and thus, phase separation. Despite their short repeat distances and multiple lamellae formation, these studies are very useful because they provide important information concerning the lipid arrangement and molecular interaction of lipids. As far as the LPP is concerned, as of this writing, very little is known about the detailed molecular arrangement of the lipid molecules in the unit cell.

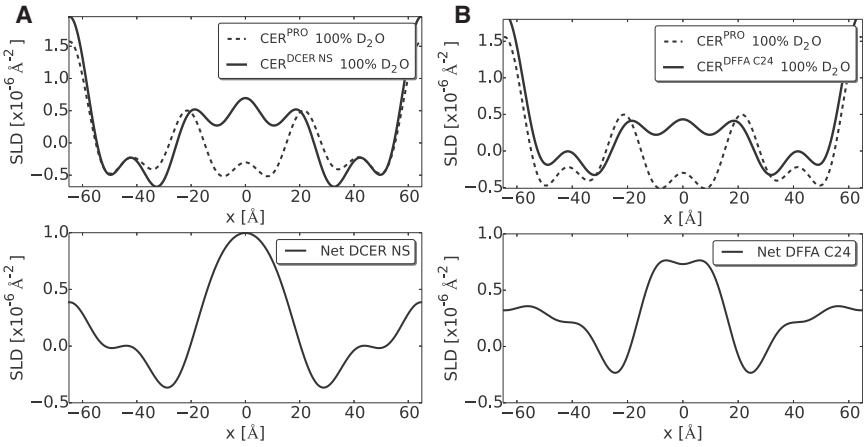

FIGURE 5 Neutron SLD profiles of the LPP model membranes in the direction normal to the unit cell surface. (*A*) Model membrane mixture for $CER^{DCER\ NS}$ and (*B*) for $CER^{DFFA\ C24}$. (*Top*, *dashed lines*) Profiles of the protiated sample. (*Top*, *solid lines*) Deuterated profiles of the model mixture. (*Bottom plots*, *solid lines*) Difference profiles were obtained by subtracting the protiated profile from the deuterated profiles, which indicate the position of the corresponding deuterated lipid molecules in the LPP unit cell.

In another study, using molecular modeling of vitreous skin section, an asymmetric arrangement of ~11 nm repeating unit of the lipid matrix has been presented (44). This contrasts with our previous findings that the LPP has a repeat distance varying between 12 and 13 nm, with a symmetric electron density distribution with four distinct headgroup regions, indicative of a three-layer arrangement in the unit cell of the LPP (31,32).

In our studies, using neutron diffraction together with isotopic (H/D) substitution, we also demonstrate a symmetric arrangement of the unit cell, based on a linear relationship between the structure factor amplitudes and the D_2O/H_2O ratios. However, for understanding the skin barrier, knowledge on the localization of the molecules within the unit cell is also crucial. In this study, our aim was to determine the localization of lipid classes in the unit cell of the LPP. In the first series of studies, we decided to focus on two highly abundant lipid subclasses in the lipid mixtures as well as in the SC (33,34), namely CER NS (C24) and FFA C24:0. To the best of our knowledge, these are the first neutron diffraction experiments reported for the localization of the lipid molecules within the unit cell of the LPP.

Choice of the CER composition in the model lipid mixtures

The natural abundance of CER EOS in the human and pig SC is ~10 mol % of the total level of CERs (33,45–48), which enables the formation of both the LPP and SPP, in human and pig SC (24,25). When examining the lipid organization of the mixtures prepared with isolated human CERs, pig CERs, or a synthetic CER mixture mimicking the pig CER composition, the phase behavior is very similar (33,49): The lipids assemble in the LPP and SPP with very similar repeat distances and the lamellar phases transform to a disordered state between 60 and 75°C. Also, in a previous study, we combined the intensities of various diffraction orders of the LPP in the diffraction curves of mixtures prepared from isolated and synthetic CERs and demonstrated that one constructed continuous Fourier transform calculated from a mixture prepared with isolated CERs fitted all the experimental Fourier factors obtained from for the various mixtures (32). Using the same set of phase angles, we showed that the Fourier factors calculated from the various orders of the diffraction curves obtained with pig SC and SC from human skin equivalents (having similar CER composition as native human SC) fitted to the same continuous Fourier transform (32). This demonstrates that not only is the phase behavior of these systems similar, but the electron density profiles within the unit cell as well. The electron density profiles serve as a fingerprint of the lipid arrangement in the unit cell and therefore it is expected that the lipid arrangement in the unit cell of the LPP in these lipid mixtures mimic closely that in SC.

In this study we wanted to form exclusively the LPP to avoid any overlap in diffraction peaks of CHOL and the diffraction peaks attributed to the SPP. Therefore, the CER EOS level was elevated in the mixture from 15 mol % (that we normally use) to 40 mol % of the CERs (50). At this CER EOS level, the lipids form only the LPP. Furthermore, when using this level, the LPP peaks are well separated from the diffraction peaks of crystalline CHOL.

Neutron diffraction pattern

In our samples the lipids form stacks of lamellae oriented approximately parallel to the silica support. Using neutron diffraction, we were able to measure nine diffraction orders attributed to the LPP with a repeat distance of 129.5 ± 0.4 Å. The seventh-order diffraction peak was not detectable in the spectra, indicating that the continuous membrane form factor is zero at this point. The diffraction pattern showed also the presence of diffraction peaks attributed to crystalline CHOL. These peaks did not interfere with those of the LPP.

Arrangement of DCER NS and DFFA C24 in the LPP unit cell

When considering the SLD profiles of CER^{PRO}, $CER^{DCER\ NS}$, and $CER^{DFFA\ C24}$, a high density is located at the boundaries of the unit cell, suggesting that the headgroups of the lipids are located at the boundaries of the unit cell whereas the hydrocarbon chains extend toward the center. Such arrangements are often observed in phospholipid bilayers (51,52). However, a second and third submaximum are also observed inside of the unit cell, located at −21 Å and +21 Å from the unit cell center, indicating that other high-density regions are also present inside of the unit cell, most probably the location of headgroups in these regions. This demonstrates that the unit cell of the LPP consists of three lipid layers that correspond to the three-layer electron density profile obtained by x-ray diffraction with high-electron-density headgroup regions at 20 Å from the center of the unit cell (32). This illustrates its believed-unique arrangement.

In the SLD profiles for both $CER^{DCER\ NS}$ and $CER^{DFFA\ C24}$, an elevated SLD is observed at the center of the unit cell. This elevated SLD is attributed to the deuterated hydrocarbon chains of CER NS or FFA (see Fig. 5), which probably partially interdigitate. The distance between the two inner headgroup regions is 42 ± 0.6 Å, which is in agreement with this interdigitation. Besides an elevated density in the center of the unit cell, in the difference SLD profiles, at the border of the unit cell, an elevation in the SLD is also observed. This suggests that a proportion of the CER NS and FFA C24 are also located at the border of the unit cell with their headgroups at the unit cell border and the hydrocarbon chains extending in the direction of the center of the unit cell.

The arrangement of the acyl chains of CER NS and FFA C24 inside the central layer in the unit cell of the LPP might be different from the arrangement of the SPP reported earlier (27,30). In the case of the SPP where the repeat distance of the unit cell is 54 Å, interdigitation of the acyl chains of CER NS and the FFA occurs and CHOL compensates for the long FFA chains that extend beyond the center of the bilayer. The position of CHOL in the LPP is not known yet. It is unlikely that the majority of CHOL is located in the central lipid layer of the unit cell of the LPP, as our study shows that the acyl chains of CER NS and FFA C24 are dominant in this layer. In a previous study (31) it was shown that CHOL is preferentially located near the outer sides of the 130 Å unit cell, and it was proposed that this unit cell contains two bilayers with CHOL asymmetrically distributed in each bilayer. This may correspond to a position of CHOL in the two outer layers of the LPP. The position of CHOL in the LPP unit cell will certainly be a subject of future studies. As of this writing, it is not known whether the CER NS is in a hairpin or in a fully extended arrangement in the LPP. If the CER NS is in a hairpin arrangement, the headgroup of the CER NS should be located very close to the two outer lipid layers at the boundary of the inner membrane headgroup regions, while in an extended arrangement there is more freedom for the acyl chains to interdigitate in order to fulfill the requirement of a layer thickness of only 42 Å. Fig. 6 displays the schematic representation of the possible arrangement of CER NS and FFA C24 in the LPP unit cell. In the figure, the CER NS and FFA C24 are shown in a symmetric hairpin arrangement.

Comparison with previously obtained x-ray diffraction results

The neutron SLD profile we obtained here (e.g., for protiated sample) is very similar to the x-ray diffraction electron

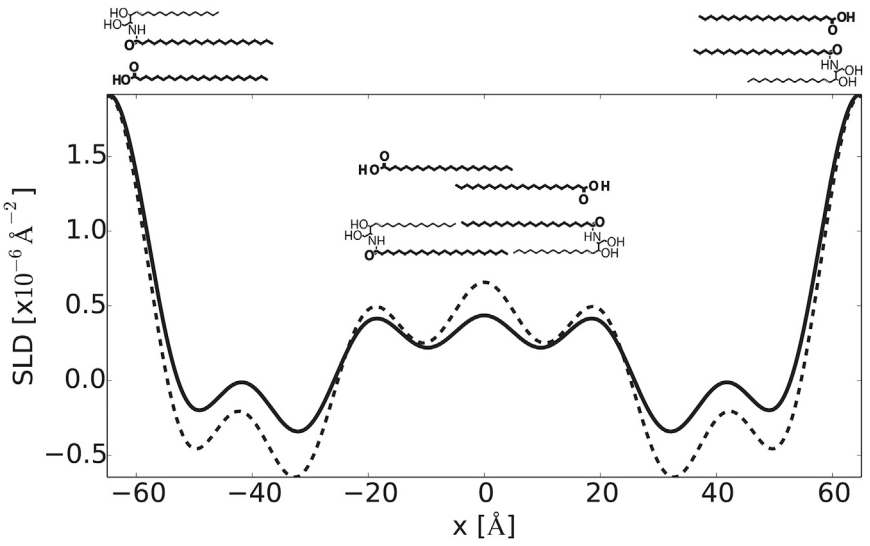

FIGURE 6 Neutron SLD profiles of $CER^{DCER\ NS}$ (*dashed line*) and $CER^{DFFA\ C24}$ (*solid line*) mixtures hydrated and measured at 100% D_2O/H_2O. A schematic of the DCER NS and DFFA C24 are also presented showing one possible arrangement within the LPP unit cell.

density profile obtained previously (32). When comparing the neutron SLD profile with the x-ray electron density profile, both profiles exhibit four distinct regions either elevated in electron density or elevated in the neutron SLD. In the electron density profile, this elevated density is located at the positions of the headgroups of the lipids, while in the neutron SLD profile of the CER^{PRO}, the maxima are related to the localization of water. When comparing these profiles, the water and lipid headgroups are located in the unit cell at very similar positions. Because the x-ray and neutron diffraction results were independently analyzed, our results demonstrate that indeed a trilayer structure of the LPP is most likely the arrangement with headgroup regions located at the unit cell border and at ~21 Å from the center of the unit cell.

CONCLUSIONS

Our studies reveal that SC lipid mixtures prepared with an elevated CER EOS level form the LPP lipid lamellae as found in human SC. The ~130 Å repeating unit of the LPP demonstrates that the arrangement of lipids involves a trilayer structure with the CER NS and FFA C24 being present mostly in the center of the unit cell with a substantial interdigitation in that region. However, in order to conceive full molecular details of the LPP, the arrangement of two other important building blocks of the LPP, namely CER EOS and CHOL, is required to fully understand the arrangement of the lipids in this phase. As of this writing, these studies are in progress.

SUPPORTING MATERIAL

Three figures and one table are available at http://www.biophysj.org/biophysj/supplemental/S0006-3495(15)00411-7.

ACKNOWLEDGMENTS

We thank the company Evonik (Essen, Germany) for their generous provision of CERs and correspondence with the Institute Laue-Langevin (Grenoble, France) for allocation of the beam time for neutron diffraction studies.

REFERENCES

1. Kiselev, M. A., N. Y. Ryabova, …, R. H. Neubert. 2005. New insights into the structure and hydration of a stratum corneum lipid model membrane by neutron diffraction. *Eur. Biophys. J.* 34:1030–1040.
2. Ruettinger, A., M. A. Kiselev, …, R. H. Neubert. 2008. Fatty acid interdigitation in stratum corneum model membranes: a neutron diffraction study. *Eur. Biophys. J.* 37:759–771.
3. Schröter, A., D. Kessner, …, R. H. H. Neubert. 2009. Basic nanostructure of stratum corneum lipid matrices based on ceramides [EOS] and [AP]: a neutron diffraction study. *Biophys. J.* 97:1104–1114.
4. Engelbrecht, T. N., A. Schroeter, …, R. H. H. Neubert. 2011. Lipophilic penetration enhancers and their impact to the bilayer structure of stratum corneum lipid model membranes: neutron diffraction studies based on the example oleic acid. *Biochim. Biophys. Acta.* 1808:2798–2806.
5. Harroun, T. A., J. Katsaras, and S. R. Wassall. 2006. Cholesterol hydroxyl group is found to reside in the center of a polyunsaturated lipid membrane. *Biochemistry.* 45:1227–1233.
6. Wiener, M. C., and S. H. White. 1991. Fluid bilayer structure determination by the combined use of x-ray and neutron diffraction. II. "Composition-space" refinement method. *Biophys. J.* 59:174–185.
7. Zaccai, G., J. K. Blasie, and B. P. Schoenborn. 1975. Neutron diffraction studies on the location of water in lecithin bilayer model membranes. *Proc. Natl. Acad. Sci. USA.* 72:376–380.
8. Worcester, D. L., and N. P. Franks. 1976. Structural analysis of hydrated egg lecithin and cholesterol bilayers. II. Neutrol diffraction. *J. Mol. Biol.* 100:359–378.
9. Franks, N. P., and W. R. Lieb. 1979. The structure of lipid bilayers and the effects of general anaesthetics. An x-ray and neutron diffraction study. *J. Mol. Biol.* 133:469–500.
10. Pebay-Peyroula, E., E. J. Dufourc, and A. G. Szabo. 1994. Location of diphenyl-hexatriene and trimethylammonium-diphenyl-hexatriene in dipalmitoylphosphatidylcholine bilayers by neutron diffraction. *Biophys. Chem.* 53:45–56.
11. Wertz, P. W., M. C. Miethke, …, D. T. Downing. 1985. The composition of the ceramides from human stratum corneum and from comedones. *J. Invest. Dermatol.* 84:410–412.
12. Ponec, M., A. Weerheim, …, P. Wertz. 2003. New acylceramide in native and reconstructed epidermis. *J. Invest. Dermatol.* 120:581–588.
13. Masukawa, Y., H. Narita, …, K. Kita. 2008. Characterization of overall ceramide species in human stratum corneum. *J. Lipid Res.* 49:1466–1476.
14. Weerheim, A., and M. Ponec. 2001. Determination of stratum corneum lipid profile by tape stripping in combination with high-performance thin-layer chromatography. *Arch. Dermatol. Res.* 293:191–199.
15. Simonetti, O., A. J. Hoogstraate, …, M. Ponec. 1995. Visualization of diffusion pathways across the stratum corneum of native and in-vitro-reconstructed epidermis by confocal laser scanning microscopy. *Arch. Dermatol. Res.* 287:465–473.
16. Boddé, H. E., I. van den Brink, …, F. H. N. de Haan. 1991. Visualization of in vitro percutaneous penetration of mercuric chloride; transport through intercellular space versus cellular uptake through desmosomes. *J. Control. Release.* 15:227–236.
17. Wertz, P. W., and B. van den Bergh. 1998. The physical, chemical and functional properties of lipids in the skin and other biological barriers. *Chem. Phys. Lipids.* 91:85–96.
18. van Smeden, J., W. A. Boiten, …, R. J. Vreeken. 2014. Combined LC/MS-platform for analysis of all major stratum corneum lipids, and the profiling of skin substitutes. *Biochim. Biophys. Acta.* 1841:70–79.
19. Park, Y.-H., W.-H. Jang, …, K.-M. Lim. 2012. Decrease of ceramides with very long-chain fatty acids and downregulation of elongases in a murine atopic dermatitis model. *J. Invest. Dermatol.* 132:476–479.
20. van Smeden, J., L. Hoppel, …, J. A. Bouwstra. 2011. LC/MS analysis of stratum corneum lipids: ceramide profiling and discovery. *J. Lipid Res.* 52:1211–1221.
21. Rabionet, M., K. Gorgas, and R. Sandhoff. 2014. Ceramide synthesis in the epidermis. *Biochim. Biophys. Actal.* 1841:422–434.
22. Holleran, W. M., M. Q. Man, …, K. R. Feingold. 1991. Sphingolipids are required for mammalian epidermal barrier function. Inhibition of sphingolipid synthesis delays barrier recovery after acute perturbation. *J. Clin. Invest.* 88:1338–1345.
23. Coderch, L., O. López, …, J. L. Parra. 2003. Ceramides and skin function. *Am. J. Clin. Dermatol.* 4:107–129.
24. Bouwstra, J. A., G. S. Gooris, …, W. Bras. 1991. Structural investigations of human stratum corneum by small-angle x-ray scattering. *J. Invest. Dermatol.* 97:1005–1012.
25. Bouwstra, J. A., G. S. Gooris, …, D. T. Downing. 1995. Lipid organization in pig stratum corneum. *J. Lipid Res.* 36:685–695.

26. Janssens, M., J. van Smeden, …, J. A. Bouwstra. 2012. Increase in short-chain ceramides correlates with an altered lipid organization and decreased barrier function in atopic eczema patients. *J. Lipid Res.* 53:2755–2766.
27. Groen, D., G. S. Gooris, …, J. A. Bouwstra. 2011. Disposition of ceramide in model lipid membranes determined by neutron diffraction. *Biophys. J.* 100:1481–1489.
28. Jennemann, R., M. Rabionet, …, R. Sandhoff. 2012. Loss of ceramide synthase 3 causes lethal skin barrier disruption. *Hum. Mol. Genet.* 21:586–608.
29. Schreiner, V., G. S. Gooris, …, J. Bouwstra. 2000. Barrier characteristics of different human skin types investigated with x-ray diffraction, lipid analysis, and electron microscopy imaging. *J. Invest. Dermatol.* 114:654–660.
30. Mojumdar, E. H., D. Groen, …, J. A. Bouwstra. 2013. Localization of cholesterol and fatty acid in a model lipid membrane: a neutron diffraction approach. *Biophys. J.* 105:911–918.
31. McIntosh, T. J. 2003. Organization of skin stratum corneum extracellular lamellae: diffraction evidence for asymmetric distribution of cholesterol. *Biophys. J.* 85:1675–1681.
32. Groen, D., G. S. Gooris, and J. A. Bouwstra. 2009. New insights into the stratum corneum lipid organization by x-ray diffraction analysis. *Biophys. J.* 97:2242–2249.
33. Bouwstra, J. A., G. S. Gooris, …, M. Ponec. 1996. Phase behavior of isolated skin lipids. *J. Lipid Res.* 37:999–1011.
34. Wertz, P. W., and D. T. Downing. 1991. Epidermal lipids. *In* Physiology, Biochemistry, and Molecular Biology of the Skin. L. A. Goldsmith, editor. Oxford University Press, New York, pp. 205–236.
35. Richard, D. 2008. http://www.ill.eu/instruments-support/computing-for-science/data-analysis/. Accessed May 2010.
36. NIST Center for Neutron Research (NCNR). 2005. www.ncnr.nist.gov/instruments/bt1/neutron.html. Accessed May 2010.
37. Nagle, J. F., and S. Tristram-Nagle. 2000. Structure of lipid bilayers. *Biochim. Biophys. Acta.* 1469:159–195.
38. NIST Center for Neutron Research (NCNR). 2014. http://www.ncnr.nist.gov/resources/activation/. Accessed: January 2011.
39. Wiener, M. C., G. I. King, and S. H. White. 1991. Structure of a fluid dioleoylphosphatidylcholine bilayer determined by joint refinement of x-ray and neutron diffraction data. I. Scaling of neutron data and the distributions of double bonds and water. *Biophys. J.* 60:568–576.
40. Jacobs, R. E., and S. H. White. 1989. The nature of the hydrophobic binding of small peptides at the bilayer interface: implications for the insertion of transbilayer helices. *Biochemistry.* 28:3421–3437.
41. Kessner, D., M. Kiselev, …, R. H. Neubert. 2008. Arrangement of ceramide [EOS] in a stratum corneum lipid model matrix: new aspects revealed by neutron diffraction studies. *Eur. Biophys. J.* 37:989–999.
42. Kiselev, M. A., E. V. Ermakova, …, A. V. Zabelin. 2014. Formation of the long-periodicity phase in model membranes of the outermost layer of skin (stratum corneum). *Crystallogr. Rep.* 59:112–116.
43. de Jager, M. W., G. S. Gooris, …, J. A. Bouwstra. 2004. Novel lipid mixtures based on synthetic ceramides reproduce the unique stratum corneum lipid organization. *J. Lipid Res.* 45:923–932.
44. Iwai, I., H. Han, …, L. Norlén. 2012. The human skin barrier is organized as stacked bilayers of fully extended ceramides with cholesterol molecules associated with the ceramide sphingoid moiety. *J. Invest. Dermatol.* 132:2215–2225.
45. Imokawa, G., A. Abe, …, A. Hidano. 1991. Decreased level of ceramides in stratum corneum of atopic dermatitis: an etiologic factor in atopic dry skin? *J. Invest. Dermatol.* 96:523–526.
46. Downing, D. T. 1992. Lipid and protein structures in the permeability barrier of mammalian epidermis. *J. Lipid Res.* 33:301–313.
47. Breiden, B., and K. Sandhoff. 2014. The role of sphingolipid metabolism in cutaneous permeability barrier formation. *Biochim. Biophys. Actal.* 1841:441–452.
48. Wertz, P. W., and D. T. Downing. 1983. Ceramides of pig epidermis: structure determination. *J. Lipid Res.* 24:759–765.
49. Bouwstra, J. A., G. S. Gooris, …, M. Ponec. 2001. Phase behavior of lipid mixtures based on human ceramides: coexistence of crystalline and liquid phases. *J. Lipid Res.* 42:1759–1770.
50. de Jager, M. W., G. S. Gooris, …, J. A. Bouwstra. 2005. Lipid mixtures prepared with well-defined synthetic ceramides closely mimic the unique stratum corneum lipid phase behavior. *J. Lipid Res.* 46:2649–2656.
51. McIntosh, T. J., S. A. Simon, …, N. A. Porter. 1984. New structural model for mixed-chain phosphatidylcholine bilayers. *Biochemistry.* 23:4038–4044.
52. Tero, R., H. Watanabe, and T. Urisu. 2006. Supported phospholipid bilayer formation on hydrophilicity-controlled silicon dioxide surfaces. *Phys. Chem. Chem. Phys.* 8:3885–3894.